Calculation and Visualization of Range of Motion of Hip Joint from MRI

Sahar Aghayan
School of Information Technology and Engineering
University of Ottawa
Ottawa, ON, Canada

Won-Sook Lee
School of Information Technology and Engineering
University of Ottawa
Ottawa, ON, Canada

***Abstract*— Femoro-Acetabular Impingement (FAI) is a hip joint disease which affects and impairs the range of hip motion during performing activities of daily living, jogging, walking, or climbing stairs due to bony abnormalities of the joint. In this research we introduce a motion simulation and visualization system which helps surgeons to analyze range of hip motions as well as to have a better communication with patients. We evaluate the maximum motion that the joint can achieve from its bony structure if the muscle and other connective tissues are perfectly trained. These goals are achieved by presenting three dimensional (3D) visualizations of motions envelopes by examining maximum possible rotation of the digital hip bones through computer-based simulation. Our computer-based simulation system estimates, analyzes and visualizes the maximum hip range of motion (ROM) for the constructed 3D bone models (femur and pelvis) that are extracted from Magnetic Resonance Images (MRI) after segmenting the bones. These tasks are accomplished first by calculating Hip Joint Center (HJC) which is center of rotation of femoral head followed by simulating hip motions with examining impingement between the femur and the acetabulum using a collision detection system. Six primary plane motions (flexion/extension, abduction/adduction and internal/external rotation) as well as various combinations of these motions and six successive movements are simulated and analyzed along with 3D visualization of estimated range of these motions. Our system by 3D visualization of motions envelopes will provide a platform to understand quicker and better the effect of bony morphology of the hip joint on the possible ROM.**

Keywords— MRI; hip joint; femoro-acetabular impingement; range of motion

I. INTRODUCTION

A massive amount of factors including biochemical, genetic, and common morphological abnormalities may lead to early Hip Osteoarthritis (OA) [1] [2] [3] especially in young and active patients such as ballet dancers and athletes. FAI is characterized as an anatomical morphology of the acetabulum and the proximal femur which causes abnormal contact at the hip joint and limits the joint rotation [4] [5]. In general, two types of FAI can be distinguished, pincer and cam FAI. The pincer FAI is characterized by overcoverage of femoral head by acetabulum [3] , or acetabulum retroversion [15]. In contrast, the cam FAI is caused by osseous bump deformity on the femoral head–neck junction [2] [3]. Often, there is a combination of both, with one type being predominant. Consequently, FAI impairs hip joint and leads limitation of movement and declines ROM [7] [8]. ROM is defined as the permitted motion of the hip joint and it is obtained from impingement-free motions. A numbers of anatomical (e.g. gender, age and ethnicity) and training-related (activity level) factors affect the maximum possible ROM [9]. For example, hip rotation degrees decrease with increasing age[9]. Some investigation show that some extreme movements increase load and consequently stress in the joint [6]. Indeed, sporting activities that require repetitive and extreme movements (e.g. dancers, gymnasts and hockey players) cause degeneration of labrum and frequent impingement between bones. Bones rub against each other causing stiffness and pain. In order to diagnose FAI, different clinical evaluations of the hip joint are employed before any operation, which includes physical hip examinations, MRI or computed tomography (CT) examinations and morphological analysis of bony structures [9]. Clinical hip examinations [20] [7] are mainly aimed to localize pain and determine joint ROM. During the examinations, different hip rotational movements are executed, for instance, internal rotation degree for flexed and adducted hip in a patient with positive "impingement test" is assessed. On the other hand, surgical operation of hip joint involves soft tissues and osseous repairs with the purpose of improvement in the clearness for hip motion. Since the hip operation can be highly invasive, it is essential that surgeon has an effective vision about the range of joint motion before operation to know exactly about the surgery strategy and minimize the risk of miss-operation.

A typical way of motion study is based on markers placement and motion capturing systems in real-life. However, it has disadvantages of being dependent and sensitive to the markers placement, skin cloth artifacts and size of the markers. In addition, it requires a specialized experimental room setting for motion capture and it is difficult and painful to obtain maximal motions. Thereby, a versatile markerless simulation of hip joint kinematics and ROM improves accuracy and efficiency of the system. Furthermore, it is difficult to isolate the effect of bone outlines out of anatomical factors such as muscles, tendon and other connective tissues which are merged in motion capture in real-life. Also various factors such as warm up and stretching exercise affect the acquired motion capture data resulting greater ROM. Therefore, we are motivated to develop a computer-assisted simulation system to digitally simulate and analyze maximum hip rotational movements from only bony morphologies of provided hip MRI

and to develop 3D visualization of maximum ROMs envelopes. A 3D simulation and visualization of patient's hip joint and its ROM can help surgeon to have a better communication with patients and it will provide a valuable insight into the understanding of hip pathology. The 3D visualization of motions envelopes provide a quick and intuitive understanding of the effect of FAI on the maximum possible range of hip motion. Therefore, the FAI patient would be able to broadly understand why she/he needs to have the surgery and how this operation can improve her/his joint mobility. It can also be used for non-FAI patients:

- To advice athletes, how big their maximum possible hip movement is to prevent impingement between the osseous anatomy of the proximal femur and the acetabulum by pushing too hard.
- To encourage not-sportive people to do more exercise to train their muscles by determining the maximum ROMs achievable with their hip bone shapes.

Despite the studies on analyzing and simulating hip kinematics and evaluating the effect of different kind of FAI on the ROM [6] [49] [5] [41], there is no much research in the area of 3D visualization of hip ROM envelope from 3D segmented MRI model. Hence, we are inspired to develop a visualization system to estimate the maximum impingement-free ROM from bony structure of the hip to evaluate the maximum possible mobility of the joint without considering the soft tissue effects.

II. METHODOLOGY

Our computer-based motion simulation and visualization system starts with segmentation of bones from MRI and construction of 3D bone models, followed by motion simulation around the calculated HJC with the control of collision detection algorithm. The motion simulation aims to compute the maximum achievable ROMs of the joint in each direction from bony outline of the joint, as well as visualization of maximum motions envelopes.

A. Construction of 3D Hip Bones

MRI of the right hip of a 37 years old Caucasian male patient with the weight of 88 kg is acquired for our experiment. The resolution of MR image is 256 pixels by 256 pixels and the thickness of each slice is 0.81mm. We use ITK-SNAP 2.4.0 software to segment the proximal femur and the pelvis bones from MRI of the patient. So, one hundred and sixty of MRI slices in format of Digital Imaging and Communications in Medicine (DICOM) files are imported into the software and segmented manually (Fig. 1) to obtain 3D point clouds of the femur and the acetabulum. After that, our segmented results are verified by a medical doctor from Ottawa General Hospital. A surface construction algorithm called the Ball-Pivoting, which is proposed by Bernardini et al. [12] is applied to incrementally build an interpolating triangulation of the acquired point clouds. This technique is efficient in terms of execution time and storage requirements and robust enough to handle the noise present in real data. Meanwhile constructed polygon meshes of femur and acetabulum may contain degenerate elements, self-intersecting or overlapping parts, surfaces holes, and many other flaws that make them not suitable for a widespread usage.

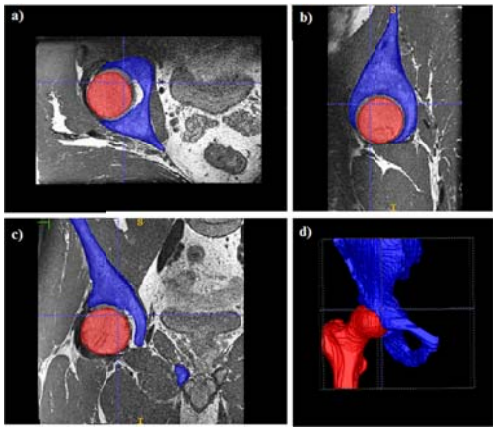

Fig. 1. a-c) segmented MRI images in axial, sagittal and coronal planes from ITK-SNAP. d) 3D constructed proximal femur (shown in red) and pelvis (shown in blue) models.

Hence, an automatic repairing procedure proposed by Attene [13] is used to remove all the aforementioned defects and transform the raw digitized meshes into single manifold and watertight triangle meshes. The complexity of obtained triangulated meshes has been reduced by Autodesk Meshmixer08 software with the purpose of lower computation and less memory cost. The constructed 3D models of the bones as shown in (Fig. 1(d)) are made of both cortical and spongy layers of bones.

B. Hip Joint Center Calculation

The subsequent articular surfaces of the hip joint, femoral head and acetabulum, are assumed to have spherical shapes as the ball-and socket joint where the femoral head is considered as the ball while the acetabulum as the socket. Hence at this stage of research, the center of hip joint is considered as the center of ball which is femoral head. Geometric calculation of the HJC exploits estimation of best sphere fitted to the sphere portion of femoral head. This center depends on the morphology of bony outline of femoral head. Accordingly, the geometric femoral head center is computed in three main steps as follow:

- 3D to 2D projection: 3D femur mesh model constructed from MRI image are converted to 2D by orthogonal projection in four different views (left/right lateral, anterior and posterior). For each anatomical view of femur, the system captures a 2D image in gray-scale.
- Image Processing: For each view, Gaussian filter has been applied to 2D gray scale image in order to remove noises and then Hough Transform method [14] has been performed in smoothen images to estimate the center and radius of circle fitted to the femoral head in 2D as shown in Fig. 2. The Hough Transform (HT) [15] is a standard method for shape recognition in digital images. There are some broad advantages in this method including robustness to noise, shape distortions and occlusions/missing parts of an object.
- 2D to 3D projection: In the last step, the 2D images have been projected back to 3D and an average center from different views has been measured.

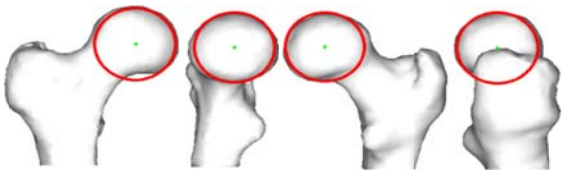

Fig. 2. Result of Hough transform in anterior, right lateral, posterior and left lateral views of a right femur model (respectively from left to right).

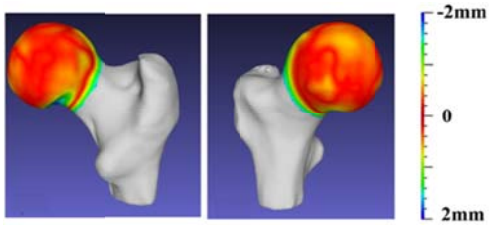

Fig. 3. Color scale of the difference from femoral head surface and fitted sphere.

In Fig. 3, a color scale is used to visualize the difference from the calculated sphere to the surface of 3D femoral head. The figure shows that the error of fitting a sphere to the femoral head surface is minor with small quantitative error.

C. Collision Detection

Simulation of hip motion requires precise collision detection [8] [10] when 3D computerized model is constructed from segmented CT, MRI or etc. While tremendous number of collision detection techniques for rigid bodies has been recommended in static and dynamic environment, we need a highly efficient collision detection algorithm to detect the real time interaction between femur and acetabulum during motion. Therefore, inspired by Cai et al. [16] and Maciel et al. [17], we implement a collision detection system to realize real-time interaction between proximal femur and acetabulum during hip motions. Detection of collision between two 3D surface models is performed in two main stages. First at the sampling phase, the quasi-spherical portions of proximal femur and acetabulum surface models are spherically sampled. Then at collision detection phase, collision has been detected based on distance difference between two sampled surface models.

1) Sampling Phase

At the sampling phase, the system gets the triangulated proximal femur and pelvis models and extracts their quasi-spherical portion based on fitting sphere to femoral head and acetabulum rim independently. Sphere fitting to the femoral head is described in the aforementioned section B. For the pelvis model, the sphere fitted to concave acetabulum is estimated based on placement of four control points (markers) (Fig. 4). From analytic geometry, we know that there is a unique sphere that passes through four non-coplanar points if, and only if, none three combinations of four points be collinear. So four control points (x_1, y_1, z_1), (x_2, y_2, z_2), (x_3, y_3, z_3), (x_4, y_4, z_4) is set up on acetabulum, three points on acetabulum rim and one on its depth as shown in Fig. 4(a). The sphere with center (X, Y, Z) and radius (R) is evaluated based on the polynomial equation as in (1).

$$(x_i - X)^2 + (y_i - Y)^2 + (z_i - Z)^2 = R^2,\ i = 1,2,3,4 \quad (1)$$

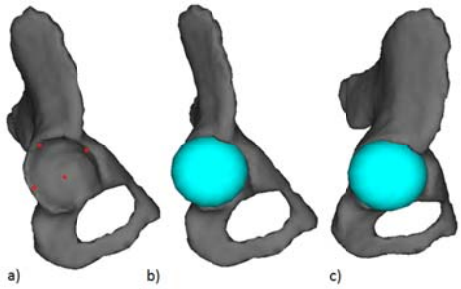

Fig. 4. Calculation of acetabulum center: a) four markers (red dots) on acetabulum is set up, three on the rim and one on its depth. b,c) Result of spherical approximation of acetabulum.

For each of the models (proximal femur and acetabulum), one bounding sphere is placed in its local coordinates centered in the center of its tightly fitted spheres with the radius, R'. Radius R' is set to be greater than R to ensure the efficiency of system in detection of anterosuperior and poster-inferior impingements. Consecutively, those triangles which are sited inside the bounding sphere are selected and listed in the table named Sampling List (SL) to be sampled. Since the hip joint is quasi-spherical, the accumulated triangles in SL tables of both mesh models (proximal femur and pelvis) are transformed to a 2D spherical grid based on (2) and (3). Therefore instead of using three parameters for indexing, two parameters are used to accelerate the computation with less complexity. Each combination of the two angle parameters Θ and $\emptyset$, in the spherical coordinates system represents a unique ray in 3D Cartesian coordinates system. With one more parameter; distance d, they produce a one-to-one correspondence to a vertex (x, y, z) in the Cartesian coordinates system.

$$x = d \sin\phi \sin\theta;\ y = d \cos\phi;\ z = d \sin\phi \cos\theta \quad (2)$$

Where $d \in [0, \infty)$, $\theta \in [0,360)$ and $\phi \in [0,180]$.

$$d = \sqrt{x^2 + y^2 + z^2};\ \theta = \tan^{-1}\left(\frac{x}{z}\right);\ \phi = \cos^{-1}\left(\frac{y}{d}\right) \quad (3)$$

Once the triangles in SL table are mapped to 2D grid, they are sampled based on rasterization and interpolation with coefficients of barycentric coordinates. The sampled points of each model are stored for further analysis in a data structure calling Look-Up table (LUT) which is a 2D array indexing by the spherical coordinate's Θ and $\emptyset$. The interpolated distance value (d_i) of the sample point in the orientation Θ_i, $\emptyset_i$ is stored in the corresponding cell of LUT ($LUT[\Theta_i][\emptyset_i] = d_i$). The size of the $LUT[\Theta][\emptyset]$ is considered as 25,927,200 ((360/0.05) * (180/0.05+1)), since the sampling precision is defined as 0.05° degree.

2) Collision Detection Phase

Each cell of LUTs indicates a unique sample point in the surface which is distinguishable by its orientations Θ and $\emptyset$. We compute the distance differences between two sampled surfaces by comparing their LUTs cells in the corresponding indices to ensure that there is a sufficient space between models. So, the LUT of acetabulum is compared to the LUT of femoral head. In general, a constant distance between two mesh models is considered as the thickness of cartilage (2mm). If distance differences between two sampled surfaces become less than the cartilage thickness, it means that there is a collision and the models are penetrating. On the other hand, if

the distances between two sampled surfaces are greater than the allowed distance, there is no collision between them. Since the LUTs of sample points are indexed same by Θ and $\emptyset$ and sample points for neighboring surfaces are congruent (same orientation); therefore, comparing those LUTs provides us exact and correct detection of impingements.

D. Hip Motion Simulation Design

The motions of constructed 3D hip bones are simulated so that the femur rotates around the computed HJC which is center of the femoral head and about the arbitrary axes while the pelvis bone is fixed. Normally hip joint undergoes six different plane-movements including flexion/extension in sagittal plane, abduction/adduction in frontal plane, and internal/external rotations in transverse plane. We simulate the motions of the hip joint at its extremity. Each movement of the hip is restricted by the collision detection algorithm associated with bony morphological constraints. The digital proximal femur rotates around HJC and stops whenever it detects collision. Then, the ROM of the hip joint in each direction is calculated and visualized for further analysis. In this research, the ROMs of the hip joint represent the maximum achievable rotational angles of the femur around the HJC. In addition to six plane-movements of the hip, successive movements (e.g. flexion with adduction) and combinational movements of the hip joint are simulated. The successive movements of the joint are simulated to analyze flexibility and extendibility of the joint when it is abducted/adducted or internally/externally rotated.

Besides, a combinational movement is simulated for the joint. A clock system is designed for the 3D femur bone in a way that, the face of the clock is projected on the transverse plane which is passed through the HJC as shown in Fig. 5. The center of clock is placed at the HJC and divides the femoral head into 12 sectors. The 12 and 6 o'clock are placed on frontal axis and the 3 and 9 o'clock are placed on sagittal axes. After that, the maximum rotational movement of the joint is performed around the clock hours hand in clockwise, from 12-6-12 o'clock (right-handed). The maximum degrees that hip can rotate around each axis (clock hours hand); restricting by the collision detection algorithm, is considered as the maximum ROMs of that o'clock.

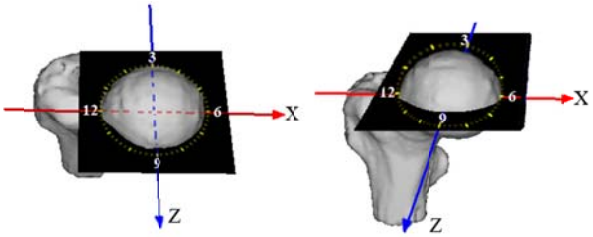

Fig. 5. Illustration of a projected clock on the transverse plane (the black square) which is passing through HJC (noted that center of clock is placed at the HJC). The left snapshot is top-view and the right is front-view. The axis Z is the front of body and the axis X is inward.

III. RESULT

A. Range of Motion Analysis

Through our computer-based motion simulation system, the upper limits of rotational angles for pair of plane-movements (flexion/extension, internal/external rotation, and abduction/adduction) about different axes are evaluated as shown in TABLE I from 3D constructed hip bones of the adult male after segmentation of MRI of the joint.

Our observation on conducted successive motions demonstrates that maximum flexion and extension rotational angles are considerably reduced per abduction and adduction motions as Fig. 6 and Fig. 7, respectively. However, this reduction is more significant for extension movement rather than flexion. The extendibility of abducted and adducted hip joint is declined to almost zero degree at the maximum degrees of abduction and adduction. But the result shows that there is still possibility of flexion when the joint is abducted and adducted. On the other hand, per rotation of the hip internally or externally (as shown in Fig. 8), the flexion remained steady at first and then in two different points, the flexion degree is dropped. In overall, it is observed that the flexibility of hip joint is diminished by rotating the joint internally or externally.

TABLE I. OUR RESULT OF ROTATIONAL DEGREES FOR SIX EXTREME PLANE-MOVEMENTS OF RIGHT HIP AROUND A FIXED HJC.

Motion	Ranges (°)
Flexion	119.8
Extension	59.4
Abduction	38.96
Adduction	36.03
Internal Rotation	35.06
External Rotation	30.2

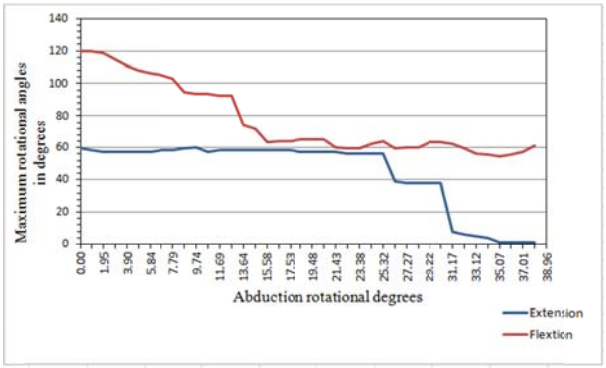

Fig. 6. Maximum rotational angles (˚) of flexion and extension in diverse abduction degrees.

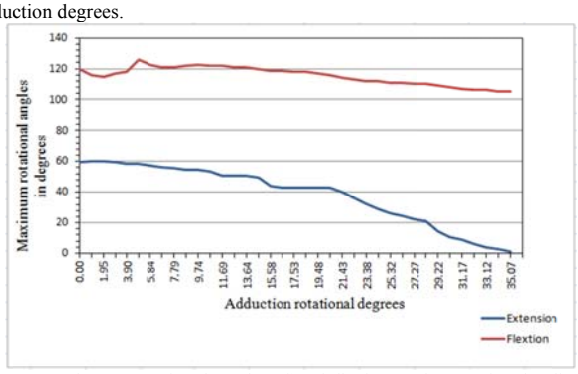

Fig. 7. Maximum rotational angles (˚) of flexion and extension in diverse adduction degrees.

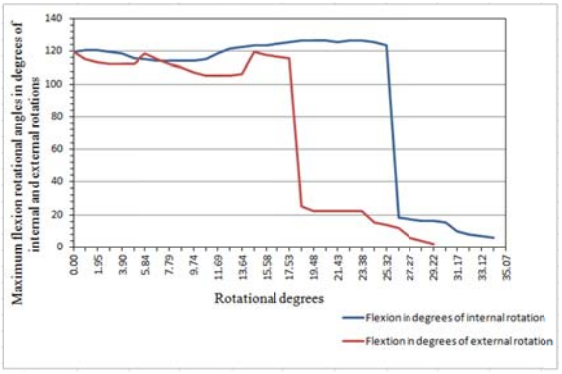

Fig. 8. Maximum flexion rotational angles (˚) of hip joint in degrees of external and internal rotations.

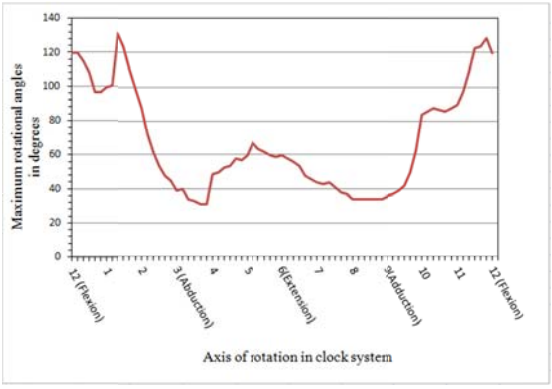

Fig. 9. Maximum rotational angle (˚) of hip joint around clock hours hand when the clock face is projected on the transverse plane that is passing through the HJC (center of clock is placed at the HJC).

The combinational movement of the hip is designed as rotation of the femur around the HJC about the rotational axes which are the clock hours hand of the projected clock on the transverse plane as illustrated in Fig. 5. Flexion, abduction, extension and adduction are occurred at rotation around 12, 3, 6 and 9 o'clock, respectively. As we expected, the maximum rotational degree is increased between flexion and abduction and the peak of maximum rotation happens between 12 o'clock to 3 o'clock and then it is declined where the abduction is occurred. At 3.8 o'clock, the trend is reached the lowest degree of rotation. Subsequently, the degree is increased slowly from 3.8 o'clock to 6 o'clock. Again between 6 o'clock and 9 o'clock is declined until the adduction is occurred. Towards the end, from 9 o'clock to 12 o'clock (adduction to flexion), the rotational degree is increased.

B. 3D Visualization of Range of Motion

After simulation of hip joint motion, the envelopes of motions are visualized in 3D space. The femur in the neutral pose is assumed as the position of a line passing from HJC to a point with coordinate data 1.0 cm, 2.0 cm and 0.0 cm, respectively as x, y and z values. The maximum ROM degrees are applied to this line to illustrate the envelope of the maximal movements of the hip joint which is computed from bony morphology of the joint. The envelope of a succesive movement is illustated in Fig. 10 which represents the flexibility and extendibility of the joint per abduction movement of hip according to the graph in Fig. 6.

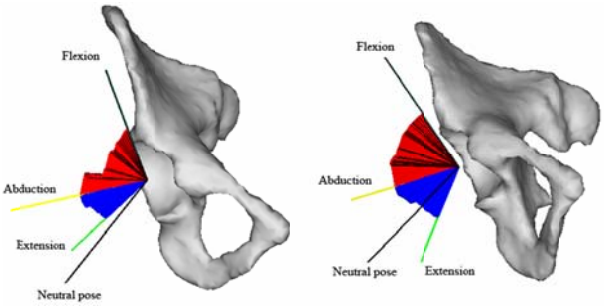

Fig. 10. Envelope visualization of Fig. 6 representing hip successive movements; abduction with flexion and extension. Blue envelope represents the extendibility of hip joint per abduction movement while the red envelope represents the flexibility of abducted joint (yellow line shows when the hip is abducted only).

The envelope of aforementioned combined motions is visualized Fig. 11. The computed ROMs from are applied to this line to illustrate the envelope of this combined motion.

IV. DISCUSION

Different plane-movement, successive and combined hip joint motions are simulated and visualized and their ROMs are analyzed. Moreover, the envelopes of a combined movement and a successive movement are visualized and further analyzed. In this research, all the conducted motions are the maximum achievable motion of the joint based on bony morphologies of the femur and the acetabulum. Although these ROMs may vary for different bone shapes, we expect to see similar trend for all type of the normal bone shapes. A hip joint with diagnosing to FAI will show different trends due to osseous abnormality of the joint. Kennedy et al. [18] assessed the effect of Cam FAI on the maximal dynamic motion of hip by using a motion capturing system. Their results revealed that maximal hip dynamic mobility decreased in internal rotation and abduction, flexed external rotation, total hip transverse ROM and total hip sagittal ROM in the FAI group compared with the healthy matched control. The visualization of ROMs envelopes can presents a better perspective of the effect of FAI variety on ROMs extents, as well as, the effect of bone shapes of the joint on the ROMs. Therefore, the joint with FAI can be distinguished from healthy hip. As our future work, more data would be collected and envelopes of these motions for healthy hips and patients diagnosed with FAI would be compared and analyzed. Our impingement detection algorithm examines the distance between the proximal femur and the acetabulum to prevent the impingement (collision) between two bone models during motion. The immense advantage of our method is its extendibility to entail the cartilage thickness information as the thickness of cartilage is varying and irregular. Additionally, since the impingement detection is based on distance difference, we can compute how close the surfaces are with providing the proximity information of the surfaces (the femur and the acetabulum).

V. CONCLUSION

In this research, we present a computer-assisted simulation system to simulate and visualize hip joint motion from MRI of the patients. The system simulates diversity of single, successive and combined hip joint motions that are controlled by a fast collision detection algorithm. During motion

simulation the proximal femur rotates around the HJC about an arbitrary axis and stops when it detects collision while an equidistant distance is considered between models as cartilage thickness. The maximum ROM degree of each conducted motion is computed through our effortless and painless motion simulation system with less error in comparison with motion capturing systems in real-life. Therefore, our motion simulation system can eventually be used before and after surgery to evaluate the effect of the applied osseous repairs on the maximal ROM degrees based on the MRI of the patient that is diagnosed with FAI. Furthermore, since the computed ROM degrees are extracted from bone shape of the joint, these degrees represent that if the patient (dancer or athlete) undertake the exercises that are involving the motions greater than these ranges, then there would be the possibility of FAI for the patient. Even for non-athlete patients, by analyzing the ROMs from bony morphological shape of the joint, the system determines whether there is a possibility of ROM improvement by undergoing physical trainings or not.

In addition, the 3D envelopes of the maximum ROM are visualized. Our 3D visualization system of the hip joint motion helps to improve communication of patient and doctor by providing more comprehensible representation of hip mobility through 3D representation of motion envelopes. Our proposed motion simulation and visualization system was welcomed by the medical doctors, particularly Orthopedics surgeons, from Ottawa General Hospital.

ACKNOWLEDGMENT

This project is funded by NSERC/CIHR CHRP grant.

REFERENCES

[1] R. Ganz, J. Parvizi, M. Beck, M. Leunig, H. Nötzli, and K. A. Siebenrock, "Femoroacetabular impingement: a cause for osteoarthritis of the hip," *Clinical orthopaedics and related research,* vol. 417, pp. 112-120, 2003.

[2] C. W. Pfirrmann, B. Mengiardi, C. Dora, F. Kalberer, M. Zanetti, and J. Hodler, "Cam and Pincer Femoroacetabular Impingement: Characteristic MR Arthrographic Findings in 50 Patients1," *Radiology,* vol. 240, pp. 778-785, 2006.

[3] M. Beck, M. Kalhor, M. Leunig, and R. Ganz, "Hip morphology influences the pattern of damage to the acetabular cartilage FEMOROACETABULAR IMPINGEMENT AS A CAUSE OF EARLY OSTEOARTHRITIS OF THE HIP," *Journal of Bone & Joint Surgery, British Volume,* vol. 87, pp. 1012-1018, 2005.

[4] R. Suppanee, M. Yazdifar, M. Chizari, I. Esat, N. V. Bardakos, and R. E. Field, "Simulating osteoarthritis: the effect of the changing thickness of articular cartilage on the kinematics and pathological bone-to-bone contact in a hip joint with femoroacetabular impingement," *European Orthopaedics and Traumatology,* pp. 1-9, 2013.

[5] S. Chegini, M. Beck, and S. J. Ferguson, "The effects of impingement and dysplasia on stress distributions in the hip joint during sitting and walking: a finite element analysis," *Journal of Orthopaedic Research,* vol. 27, pp. 195-201, 2009.

[6] C. Charbonnier, F. C. Kolo, V. B. Duthon, N. Magnenat-Thalmann, C. D. Becker, P. Hoffmeyer*, et al.*, "Assessment of Congruence and Impingement of the Hip Joint in Professional Ballet Dancers A Motion Capture Study," *The American Journal of Sports Medicine,* vol. 39, pp. 557-566, 2011.

[7] C. Charbonnier, N. Magnenat-Thalmann, C. D. Becker, P. Hoffmeyer, and J. Menetrey, "An integrated platform for hip joint osteoarthritis analysis: design, implementation and results," *International journal of computer assisted radiology and surgery,* vol. 5, pp. 351-358, 2010.

[8] T. C. Chang, H. Kang, L. Arata, and W. Zhao, "A pre-operative approach of range of motion simulation and verification for femoroacetabular impingement," *The International Journal of Medical Robotics and Computer Assisted Surgery,* vol. 7, pp. 318-326, 2011.

[9] D. J. Berry and J. Lieberman, *Surgery of the Hip* vol. 2. Elsevier Health Sciences, 2012.

[10] M. Teschner, J. Richolt, R. Kikinis, and B. Girod, "Computer-assisted analysis of hip joint flexibility," *Proc. of Image and Multidimensional Digital Signal Processing IMDSP,* vol. 98, pp. 63-66, 1998.

[11] S. J. Piazza, A. Erdemir, N. Okita, and P. R. Cavanagh, "Assessment of the functional method of hip joint center location subject to reduced range of hip motion," *Journal of Biomechanics,* vol. 37, pp. 349-356, 2004.

[12] F. Bernardini, J. Mittleman, H. Rushmeier, C. Silva, and G. Taubin, "The ball-pivoting algorithm for surface reconstruction," *Visualization and Computer Graphics, IEEE Transactions on,* vol. 5, pp. 349-359, 1999.

[13] M. Attene, "A lightweight approach to repairing digitized polygon meshes," *The Visual Computer,* vol. 26, pp. 1393-1406, 2010.

[14] M. Cao, C. Ye, O. Doessel, and C. Liu, "Spherical parameter detection based on hierarchical Hough transform," *Pattern recognition letters,* vol. 27, pp. 980-986, 2006.

[15] V. Leavers, "Which hough transform?," *CVGIP: Image understanding,* vol. 58, pp. 250-264, 1993.

[16] D. Cai, W.-S. Lee, C. Joslin, and P. Beaulé, "Rapid Impingement Detection System with Uniform Sampling for Ball-and-Socket Joint," in *Recent Advances in the 3D Physiological Human*, ed: Springer, 2009, pp. 179-192.

[17] A. Maciel, R. Boulic, and D. Thalmann, "Efficient collision detection within deforming spherical sliding contact," *Visualization and Computer Graphics, IEEE Transactions on,* vol. 13, pp. 518-529, 2007.

[18] M. Kennedy, M. Lamontagne, and P. Beaule, "The effect of cam femoroacetabular impingement on hip maximal dynamic range of motion," *Journal of Orthopedics,* vol. 1, pp. 41-50, 2009.

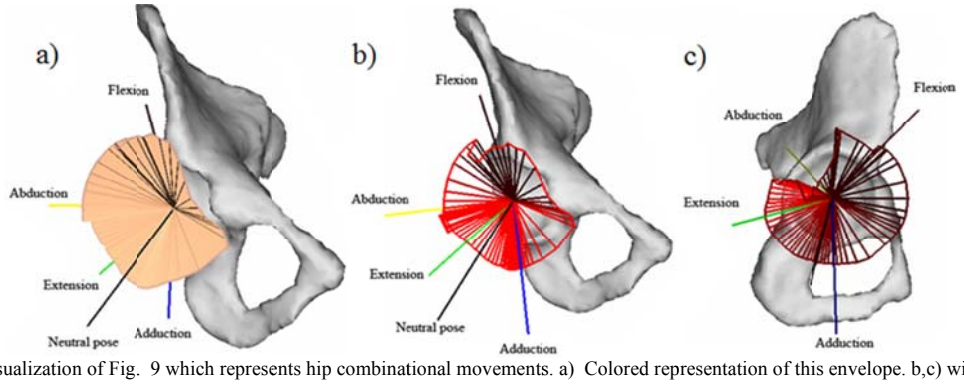

Fig. 11. Envelope visualization of Fig. 9 which represents hip combinational movements. a) Colored representation of this envelope. b,c) wired representation of the envelope, from different views.